Chemical imaging of structured SAMs with a novel SFG microscope

Dominik M.P. Hoffmann*, Klaus Kuhnke, and Klaus Kern
Max-Planck-Institut für Festkörperforschung Stuttgart, Germany

ABSTRACT

We present a newly developed microscope for sum frequency generation (SFG) imaging of opaque and reflecting interfaces. The sample is viewed at an angle of 60° with respect to the surface normal in order to increase the collected SFG intensity. Our setup is designed to keep the whole field of view (FOV) in focus and to compensate for the distortion usually related to oblique imaging by means of a blazed grating. The separation of the SFG intensity and the reflected visible beam is accomplished by a suitable combination of spectral filters. The sum frequency microscope (SFM) is capable of in-situ chemically selective imaging by tuning the IR-beam to vibrational transitions of the respective molecules. The SFM is applied to imaging of structured self-assembled monolayers (SAM) of thiol molecules on a gold surface.

Keywords: Microscopy, sum frequency generation, oblique imaging, chemical contrast, chemical imaging, nonlinear optics

1. INTRODUCTION

Within the last two decades the progress in nonlinear optics was made possible mainly by the development of laser sources that provide light with sufficiently high power density to observe higher order optical effects. Nowadays numerous nonlinear optical methods are used in various fields like surface science and biochemistry. Much effort has been made recently to combine the specific advantages and properties of nonlinear spectroscopic techniques with imaging methods. Examples are the increasing number of second harmonic generation (SHG) microscopes, coherent anti-Stokes Raman spectroscopy (CARS) microscopy[1] and a sum frequency generation microscope for transparent samples[2]. As the underlying processes involve more than one photon all these techniques have in common that the lateral resolution is enhanced in comparison to the equivalent linear process[3]. Also first results in near field sum frequency generation[4-6] have been reported.

Amongst possible nonlinear optical processes especially those of second order, like SHG and SFG, provide high interface specificity[7]. For sum frequency generation two laser pulses, typically one with a fixed visible frequency ω_{vis} and another with a tunable IR frequency ω_{IR}, are overlapped in time and space on a sample. At high intensities I_{vis} and I_{IR} this results in a nonlinear polarization P, which has contributions at the sum of the frequencies ω_{SFG}. This nonlinear polarization leads to the emission of SFG light with intensity I_{SFG}, which is proportional to the square of the absolute value of the second order nonlinear susceptibility $\chi^{(2)}{}_{tot}$**:

$$I_{SFG} \propto \left|P(\omega_{SFG} = \omega_{vis} + \omega_{IR})\right|^2 \propto \left|\chi^{(2)}_{tot}\right|^2 I_{vis} I_{IR} \quad . \tag{1}$$

In the dipole approximation, this process is absolutely interface-specific for centro-symmetric samples or media. Even for non centro-symmetric samples it has been demonstrated that interface sensitivity remains. As the efficiency of vis-IR sum frequency generation is low, the corresponding laser pulses have to be focused close to the damage threshold of the sample under investigation. The SFG signal is resonantly enhanced when the IR wavelength is tuned to a vibrational transition $|0\rangle \rightarrow |\omega\rangle$ that is both Raman and IR active. Thus vis-IR-SFG is a technique for in-situ vibrational

* d.hoffmann@fkf.mpg.de

** $\chi^{(2)}{}_{tot}$ actually is a tensor. For a given beam geometry it can be reduced to an effective second order nonlinear susceptibility, which is a complex quantity. In the following this effective second order nonlinear susceptibility will be simply denoted as second order nonlinear susceptibility or nonlinear susceptibility.

spectroscopy at interfaces and surfaces. Chemical information on an interface can be obtained by tuning the IR to specific vibrational transitions.

A sum frequency microscope (SFM) projects the SFG light generated at an interface by the incident beams onto a CCD camera. It thus provides a map of the SFG efficiency of the interface. The SFM can provide information about areas with different degrees of ordering. As the spatial resolution is limited by the wavelength of the sum frequency light, being typically in the visible range, an SFM delivers information from the IR spectral region with potential sub-μm spatial resolution. Furthermore, it offers a time resolution determined by the employed laser beams. A further application could be the simultaneous measurement of samples, i.e. combinatorial SFG spectroscopy.

In spite of these attractive properties only one far field SFM has been reported so far[2], which is applicable only to transparent samples. We plan to examine adsorbates on opaque surfaces as metals and semiconductors. Therefore we developed a different setup. The design of the SFM poses two major difficulties: 1) The SFG intensity originating from an interface is proportional to the square of the corresponding Fresnel factors[8] being a function of the angles θ_{vis}, θ_{IR}, θ_{SFG} of the three laser beams with respect to the surface normal and of their polarizations. If a metal sample is viewed at an angle $\theta = 0°$, i.e. parallel to the surface normal, the Fresnel factor and thus the SFG intensity will be extremely low. In order to obtain a maximum SFG intensity, the visible and the IR pulses have to illuminate the sample at an angle of about $\theta = 60°$ and the sample is viewed at a similar angle. In a standard microscope, the numerical aperture (NA) would have to be small in order to obtain a high depth of field (DOF). A large DOF is necessary to keep the whole field of view (FOV) in focus. However, a small NA results in a low spatial resolution. A conventional microscope cannot give satisfying results because both DOF and NA cannot be maximized at the same time. 2) Due to wave vector conservation in the sum frequency generation process at the surface the reflected visible beam and the generated SFG intensity are in very close angular vicinity. The visible beam is about 15 orders of magnitude more intense than the SFG light and it has to be suppressed while as much SFG intensity as possible should be transmitted.

In the following section we describe our setup, which solves these problems. In section 3 the study of structured self-assembled monolayers with an SFM shows that taking SFG images at different wavelengths and by exploiting electronic and chemical contrast mechanisms can retrieve information on different parts of adsorbed molecules.

2. SUM FREQUENCY MICROSCOPE

The visible and the IR beam are produced by a laser system with 35 ps pulses and 20 Hz repetition rate. A visible beam at a fixed wavelength $\lambda = 532$ nm (2^{nd} harmonic of the Nd:YAG fundamental at 1064 nm) is mixed on the sample with an IR beam originating from a narrow band optical parametric generator and amplifier (OPG/OPA) setup similar to the one described in reference 9. The IR wavelength can be tuned between 4000cm^{-1} ($\lambda = 2{,}5$ μm) and 1000cm^{-1} ($\lambda = 10$ μm), a major region for vibrational transitions. The microscope setup is initially optimized for spectroscopy in the interval between $\lambda = 2.9$ μm and $\lambda = 4$ μm, i.e. for SFG wavelengths between $\lambda = 450$ nm and $\lambda = 470$ nm. The interval can be extended or shifted to different regions in the IR spectrum by exchanging some filters and a grating.

Figure 1 shows the setup of the microscope in a reflection configuration. The planned SFG experiments usually require the visible, the IR and the SFG beams to be p-polarized. The visible beam at $\lambda = 532$ nm and the IR beam illuminate the sample at an angle of about 60° in order to maximize the SFG output. The generated 0^{th} order SFG beam (dashed line in Fig. 1) leaves the sample at an angle close to the reflected visible beam. A short pass interference filter (Linos Photonics) in front of the first objective already attenuates the visible beam by 4 orders of magnitude. Thus damage of the objectives is avoided.

While in SFG spectroscopy only the 0^{th} order SFG beam is detected, in a microscope also the diffracted orders have to be collected by an objective. A conventional microscope cannot be used for the reasons given above and the approach is different: A 1:1 intermediate image is projected by the camera objectives onto the grating. As the lens plane is tilted with respect to the object plane (sample), the image plane (grating) must be tilted such that all three planes have a common intersection line. This is known as Scheimpflug's principle. A 50x microscope, which is aligned perpendicular to the surface of the grating, magnifies the intermediate image. A more extended theoretical treatment on this configuration is found in reference 10.

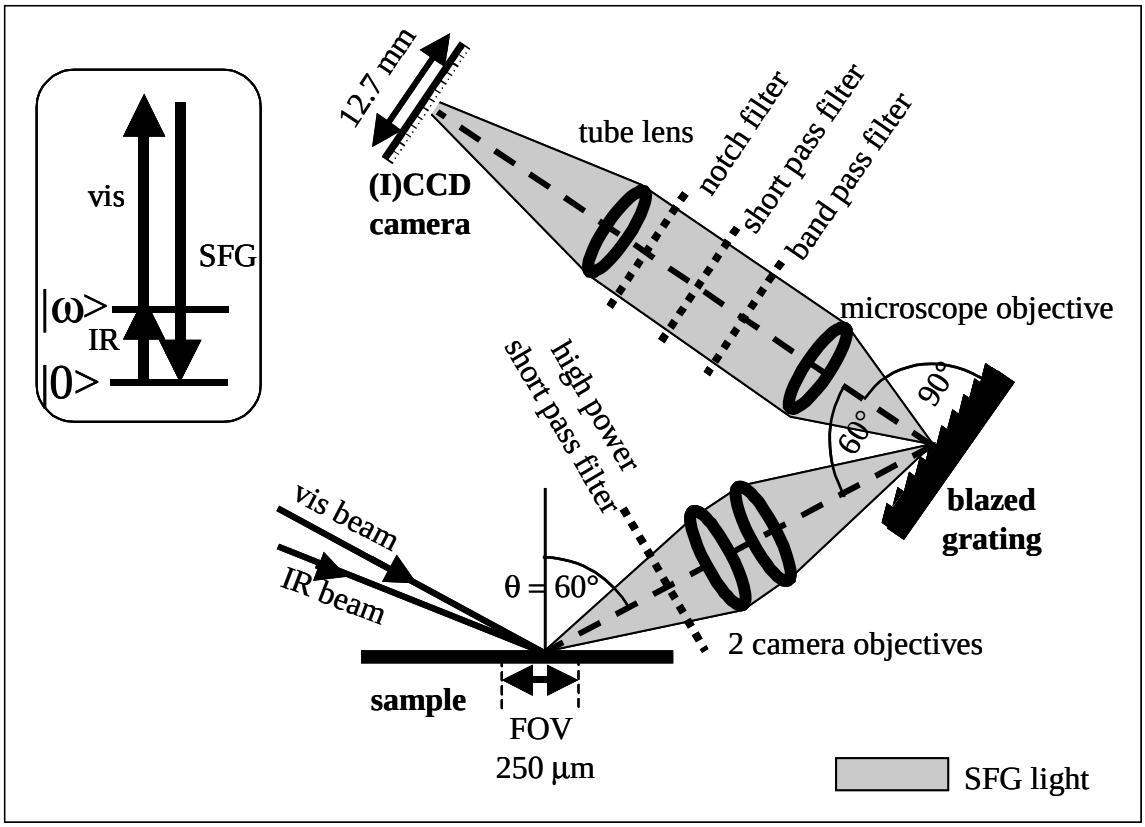

Figure 1: Optical setup of the sum frequency microscope. For clarity the reflected visible and IR beams have been omitted. The first stage forms a 1:1 intermediate image on the grating. The image is subsequently enlarged by a 50x microscope and recorded by a scientific grade CCD camera. Inset: Term scheme of vis-IR-SFG: Two incoming photons at the energy ω_{vis} and ω_{IR} are mixed by the nonlinear susceptibility $\chi^2(\omega_{vis}, \omega_{IR}, \omega_{vis} + \omega_{IR})$. An SFG photon at $\omega_{SFG} = \omega_{vis} + \omega_{IR}$ is emitted. The SFG signal is resonantly enhanced when the IR energy matches a real transition $|0\rangle \rightarrow |\omega\rangle$, which is both Raman and IR-active.

The key element of the setup is the grating, which has to be placed in the image plane of the camera objectives and in the object plane of the microscope. Its blaze angle is 30°. Light originating from one point of the sample is reflected into the aperture of the microscope. Additionally, the grating constant has to be chosen such that SFG light from the sample is diffracted in first order into the microscope objective. Measuring at about 450 nm SFG wavelength, we have selected an 1800 lines/mm grating with a 500 nm blaze (Jobin-Yvon). The 1:1 imaging system consists of two f = 58 mm, f/1.2 Noct-Nikkor objectives with aspherical lenses (Nikon). The 50x microscope is an infinity corrected LPlan 50x / 0.45 objective with 17 mm working distance and a tube lens (Nikon).

The microscope is shielded from ambient light by a box of black cardboard. There is, however, stray light coming directly from the imaged area, namely the reflected visible beam and fluorescence light. Therefore we inserted three filters between the microscope objective and the tube lens: A holographic notch filter (center 532 nm, FWHM 10 nm, Kaiser Optical Systems Inc.), an interference band pass filter (450 nm, FWHM 40 nm, L.O.T.-Oriel) and an interference short pass filter (edge 510 nm, Omega Optical Inc.). Fig. 2 shows the absorption curve of this combination, which is obtained by adding up single filter absorption measurements. This filter combination suppresses the visible beam at λ = 532 nm by more than 20 orders of magnitude and transmits ca. 30 % of the SFG signal at λ = 450 nm.

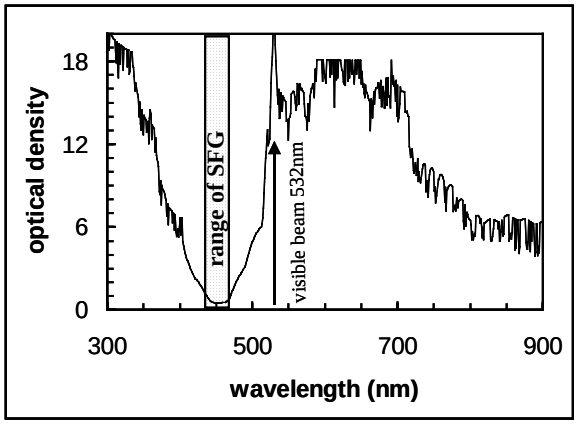

Figure 2: Absorption curve of the four-filter-combination discussed in the text. The curve is the sum of four absorbance curves measured for the individual filters. Optical densities larger than 5 may be underestimated due to the limited sensitivity of the spectrometer.

The low SFG signal requires the use of a high quantum efficiency detector. We chose a back-thinned, liquid nitrogen cooled CCD camera built by Roper Scientific. The SITe chip has 512 x 512 pixels of (24 x 24) μm^2 area each, i.e. at a magnification of 50x each pixel corresponds to 0.5 μm on the sample.

Figure 3: Linear optical image: Pattern with 180 line pairs/mm imaged at λ = 450nm. The vertical resolution is better than the horizontal one.

The SFM has a field of view of 240 x 240 μm^2 that is completely in focus. This is non-trivial because one side of the FOV is about 200 μm closer to the objective than the other. The magnification in the plane of incidence (which is the drawing plane in Fig. 1) is 51.1 (±0.5) and perpendicular to that plane it is 50.3 (±0.5). The error corresponds to the uncertainty of one pixel. Within this precision the magnification is constant within the whole FOV and in all directions. This means that the setup removes the distortion usually related to oblique imaging. The experimentally determined resolution according to the Rayleigh criterion is 4.9 μm within the plane of incidence. Perpendicular to this plane it is 3.1 μm. This anisotropic behavior is shown in Fig. 3. The horizontal lines are resolved perfectly, while the resolution limit has been almost reached for the vertical lines. Both resolutions values do not correspond to the diffraction limit values. We found that the experimental resolution is determined by the aberrations of the two camera objectives used for the 1:1 imaging. A more extensive characterization of the SFM can be found in a forthcoming paper[11].

The anisotropy in resolution follows from the oblique imaging. A simulation (Fig. 4) shows this for point-like structures. The object consists of light emitting points in the object plane O. The light amplitude can be calculated for each point of the lens. The lens is assumed to be perfect. The integral over the lens plane was replaced by a discrete sum over 2000 points randomly distributed at the lens position (Fig 4.a). The first simulation shows the image in the plane perpendicular to the optical axis (A). The points on the vertical line in the central FOV are in focus. They are broadened by diffraction due to the finite lens aperture. Points closer to or further away from the objective are out of focus. Fig. 4b(B) shows the simulation for the Scheimpflug configuration we use in the SFM. The whole field of view stays in focus. The anisotropic resolution leads to an elliptic diffraction pattern of the single points. As expected, the ratio of the resolution in the simulation is equal to cos ($\theta = 60°$) = 0.5. The experimental result is 0.6, which is in fair agreement. The simulation is based on a diffraction-limited system. Introducing spherical aberrations of the lens in the simulation reduces the resolution but leads to a corresponding elliptic point spread function.

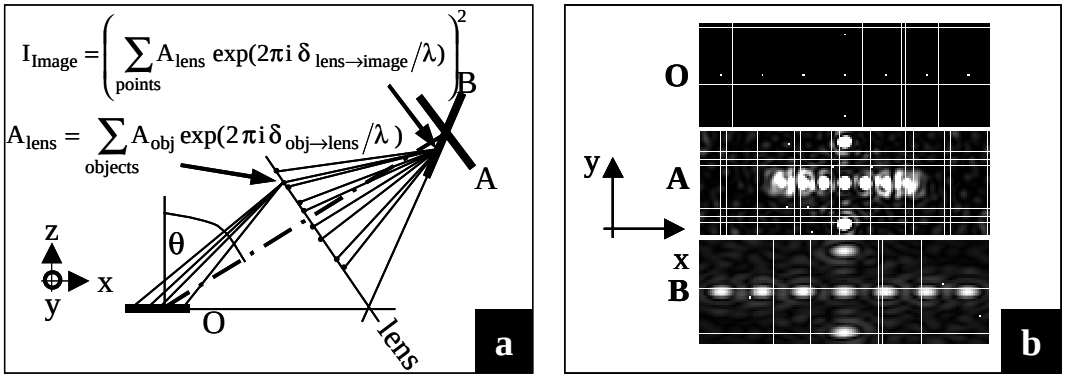

Figure 4: a) Model of anisotropic resolution in the 1:1 imaging process: b) (O) object plane, (A) calculated intensity in a plane perpendicular to the optical axis, (B) calculated image in the plane of the grating

Measurement times for the SFM depend critically on the desired signal-to-noise ratio (SNR). Main sources of noise in the setup[11] are the read-out noise of the CCD electronics, cosmic ray events on the CCD chip and residual ambient light. Therefore we extended the SFM and added an image intensifier based on a Gen II micro channel plate (MCP). The intensifier is coupled to the CCD chip by a tandem lens. The electron gain is about 800 at usual operation conditions. The read-out noise and the cosmic ray events are negligible. The image intensifier is operated in a gated mode: Triggered by the laser, the voltage is applied between the cathode and the MCP for 100 ns per pulse. For our 20 Hz laser system the residual ambient light is reduced by a factor of 1s/(20 x 100 ns) = 5 x 10^5. However, the intensifier has a 7 times lower quantum efficiency for the SFG photons when compared to the CCD chip. The point-spread-function (PSF) of the image intensifier differs from photon to photon. The varying intensity of the PSF does not matter, if the number of photons is sufficient. The spatial spread does hardly influence the resolution, as will be shown below. Thus the choice between the CCD and the ICCD configuration depends only on the SFG intensities per pixel, and therefore on the samples. All measurements shown in the following were taken with the intensified CCD camera (ICCD). The raw data have been divided by a flatfield, i.e. by the linear optical image (λ=450nm) of a blank surface. This removes the vignetting due to the coupling lenses between MCP and CCD chip. The flatfield correction also reduces most of the flaws caused by inhomogeneties of the employed optical filters.

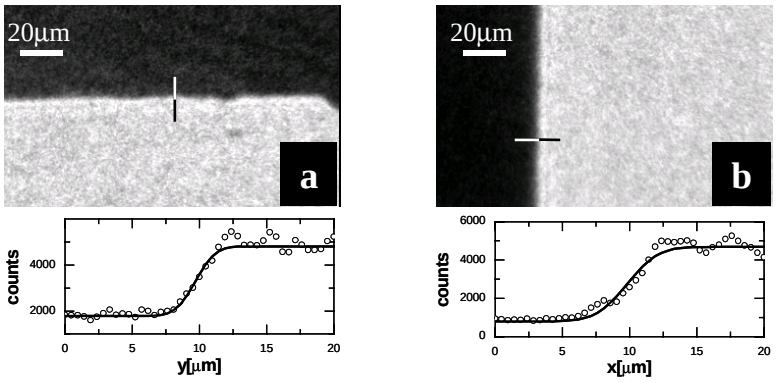

Figure 5: Linear optical images (λ = 450 nm) of
a) a horizontal edge of GaAs. The cross-section corresponds to the line drawn in the image. Vertical resolution: 3.2 µm
b) a vertical edge of GaAs. Horizontal resolution: 5.1 µm

Fig. 5a shows a linear optical image (λ = 450 nm) of a horizontal edge of GaAs. GaAs can be cut by breaking it along preferred crystallographic directions. The edges are known to be sharp on a sub-µm scale. The image has been recorded

with the intensified CCD camera. Below the image the line indicated in the image is plotted. The vertical resolution is evaluated to be 3.2 μm. The horizontal resolution (Fig 5b) is 5.1 μm. This is in good agreement with the results obtained without image intensifier. Thus the MCP does not reduce the spatial resolution significantly. The resolution is still limited by the camera objectives used for the 1:1 optics.

3. CHEMICAL IMAGING

3.1. Self-assembled monolayers

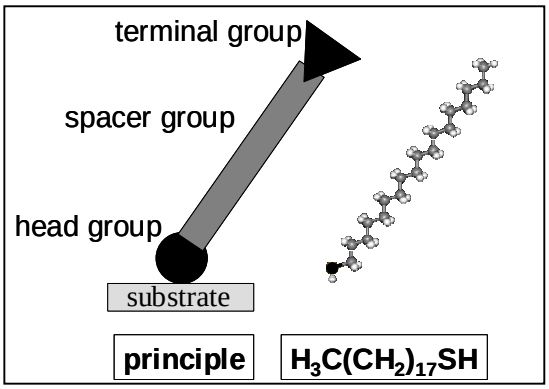

Figure 6: Scheme of a molecule that can form a self-assembled monolayer (SAM). Molecular structure of a C18 thiol

SAMs are the object of intensive research. They are formed by chemisorption of molecules, which consist of three building blocks (Fig. 6 left): The head group binds the molecule to the substrate. The spacer group stabilizes the monolayer and is important for its order and compactness. Its length combined with the orientation defines the distance of the terminal group from the substrate. The terminal group can allow for modification of surface properties. This can be used for tailoring the chemical behavior of a surface for specific applications. A carboxyl group, for example, makes the surface hydrophilic while a methyl group makes it hydrophopic. One way of producing homogeneous self-assembled monolayers is the immersion of a suited substrate in a solution that contains the molecules described before. Micro-contact printing is another technique that has been proven to be an efficient method for patterning SAM monolayers down to sub-μm lateral dimensions[12]. An overview over SAMs can be found in the references 13 and 14.

Organothiolates on Au (111) are a widely studied class of SAMs. We chose the alkanethiol $H_3C(CH_2)_{17}SH$ (short: C18 (thiol)), (Fig. 6 right) as a model system to demonstrate chemical imaging. The thiol group forms a strong S-Au bond to the gold substrate. The spacer consists of 17 methylene(-CH_2-) units. A methyl(-CH_3) group terminates this chain. C18 is known to form well-ordered, dense and stable monolayers. The molecules are tilted by ca. 30° with respect to the surface normal of a Au (111) substrate due to the van-der-Waals forces between the CH_2 chains[15].

3.2 Sample preparation

The Au substrates are prepared by evaporating a 200 nm thick gold film onto a 2 nm thick Cr layer on glass. These films are polycrystalline with preferential Au(111) surface orientation. Each substrate is flame-annealed before the C18 is adsorbed. The laterally structured SAMs are made by means of micro-contact printing. A fresh and thoroughly cleaned flat stamp of polydimethylsiloxane (PDMS) is exposed for 30 s to a 1 milli-molar solution of C18 in ethanol. After it has been blown dry under a stream of Argon for at least 30 s, the stamp is brought into contact with the substrate for 60 s. Finally the stamp is removed and the sample is rinsed with ethanol in order to remove excessive C18 molecules. The sample is mounted in the SFM. By taking linear images under narrow band 450 nm illumination we adjusted the microscope focus; small Au defects were helpful.

3.3 Electronic and vibrational contrast

The second order nonlinear susceptibility $\chi^{(2)}_{tot}$ of the surface consists of three components. $\chi^{(2)}_{Au}$ originates from the Au substrate. This component is comparatively large for the wavelengths we use due to an interband transition in the gold substrate[16] and it changes by the amount $\chi^{(2)}_{Au\text{-}S}$ upon thiol adsorption. $\chi^{(2)}_{Au\text{-}S}$ is a function of the thiol coverage Θ[17]. Both terms are nonresonant in the IR energy. Therefore they can be treated together as $\chi^{(2)}_{nr}$. The nonlinear susceptibility $\chi^{(2)}_{ads}$ of the adsorbed C18 thiol is described by a vibrational resonant nonlinear susceptibility $\chi^{(2)}_{vib}$, which assumes an important value whenever the IR beam is resonant with a Raman and IR active vibrational transition. The nonresonant nonlinear susceptibility of C18 thiol can be neglected when compared to the one of gold. We have

$$\chi^{(2)}_{tot} = \chi^{(2)}_{Au} + \chi^{(2)}_{Au-S}(\Theta) + \chi^{(2)}_{ads} \cong \chi^{(2)}_{nr} + \chi^{(2)}_{vib} \quad , \qquad (2)$$

with

$$\chi^{(2)}_{vib} \propto \sum_q \frac{A_q}{\omega_q - \omega_{IR} + \Gamma_q} \quad . \tag{3}$$

ω_q denotes the energy of the q^{th} vibrational transition, A_q the corresponding transition matrix element and Γ_q its width. The SFG signal is proportional to the square of the second order nonlinear susceptibility $\chi^{(2)}_{tot}$:

$$I_{SFG} \propto \left|\chi^{(2)}_{tot}\right|^2 = \left|\chi^{(2)}_{nr} + \chi^{(2)}_{vib}\right|^2 \approx \left|\chi^{(2)}_{nr}\right|^2 + 2\left|\chi^{(2)}_{nr}\right|\left|\chi^{(2)}_{vib}\right|\cos\varphi \quad . \tag{4}$$

An SFG spectrum of a C18 thiol SAM on Au measured with our SFM is shown in Fig. 7. The spectrum is normalized to the nonresonant baseline that corresponds to $\chi^{(2)}_{nr} = \chi^{(2)}_{Au} + \chi^{(2)}_{Au\text{-}S}$. Within the region of C-H vibrations three strong resonances are found. They are attributed to methyl stretching vibrations. The symmetric methyl stretch is split up by a Fermi resonance into two components r^+_aFR (2878±3cm^{-1}) and r^+_bFR(2938±3cm^{-1}). The in-plane and out-of-plane asymmetric stretching vibrations of the methyl group cannot be separated in our spectrum: r^-(2968±3cm^{-1}). As the nonlinear susceptibilities are complex quantities, the phase angle φ (~ π) between $\chi^{(2)}_{nr}$ and $\chi^{(2)}_{vib}$ causes the resonances to appear as negative peaks. The absence of resonant features related to the methylene group (e.g. at 2918 cm^{-1}) indicates that the SAM is well ordered and that the molecules are predominantly in an all-trans configuration[18].

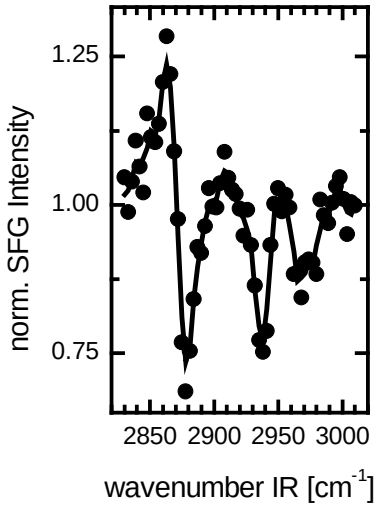

Figure 7: SFG spectrum of a printed C18 thiol SAM on Au. Points are measured data, the solid line is a smoothed curve averaged over 3 data points

Fig. 8a is a linear optical image of a Au substrate taken under narrow band 450 nm illumination. In the figure the line indicates the border of an area on which C18 thiol was printed. Fig. 8b shows an SFG image taken at the same position. An average intensity of about 20 photons per μm^2 in the C18 area has been detected during an acquisition time of 80 min. At this low intensity photon noise is significant as can be seen in the SFM images. In the linear optical image no difference appears between the covered Au and the uncovered one, as can be expected. A contrast, however, is observed in an SFG image (Fig. 8b) with an IR wavenumber of 2835cm^{-1}, which is nonresonant with any vibrational resonance of the thiolate. Due to the bonding of the sulfur to the substrate the nonlinear susceptibilities in the both areas differ by $\chi^{(2)}_{Au\text{-}S}$ (eq.(2)). This change can be correlated to the C18 coverage Θ[16]. The area covered by C18 thiolate exhibits an SFG intensity that is about 33% lower than the intensity of the clean Au area. Fig. 8c shows an SFM image of the same region at a wavenumber of 2878cm^{-1}, i.e. in resonance with the CH_3 symmetric stretching mode. The SFG intensity in the C18 thiolate region has decreased by a further 26% when compared to the nonresonant image. This agrees well with the spectrum (Fig. 7). The contrast between clean and thiolate covered Au surface is thus enhanced by the contrast due to the methyl vibration. Based on eq. (4) we define a vibrational contrast $2\cos(\varphi)\chi^{(2)}_{vib}$ that can be deduced from the resonant and nonresonant intensities I_{res} and I_{nr}:

$$2\cos(\varphi)\chi^{(2)}_{vib} \propto \frac{I_{res} - I_{nr}}{\sqrt{I_{nr}}} \tag{5}$$

Fig. 8d shows the vibrational contrast calculated with eq. (5) using the measurements displayed in Fig. 8b and 8c. The dark regions represent the presence of methyl groups in an upright orientation (dark because cos (φ) ~ -1). The bright regions correspond to their absence. The ripples, which are most obvious in the bright areas are probably due to the interference filters. If the thiolate contained no methyl groups or if their axis were oriented parallel to the surface, the image would exhibit no contrast. Fig. 8d, however, shows a contrast of about -20% when compared to $\chi^{(2)}_{Au}$. $\chi^{(2)}_{Au}$ has been normalized to 1 before applying eq.(5). That is in agreement with the contribution of the symmetric stretching mode in the vibrational spectrum (Fig. 7). The edge of the adsorbed thiolate can clearly be discerned. On the left part of

this border it appears, however, that the region of methyl groups extends further on the Au substrate than the chemisorbed thiolate, which is mapped by the electronic contrast (Fig. 8b). This suggests that the dark region below the border indicates an impurity on the substrate. We can, however, not exclude that the spot is due to the illuminating beams, which may exhibit slightly different intensity distributions in Figs. 8b and 8c.

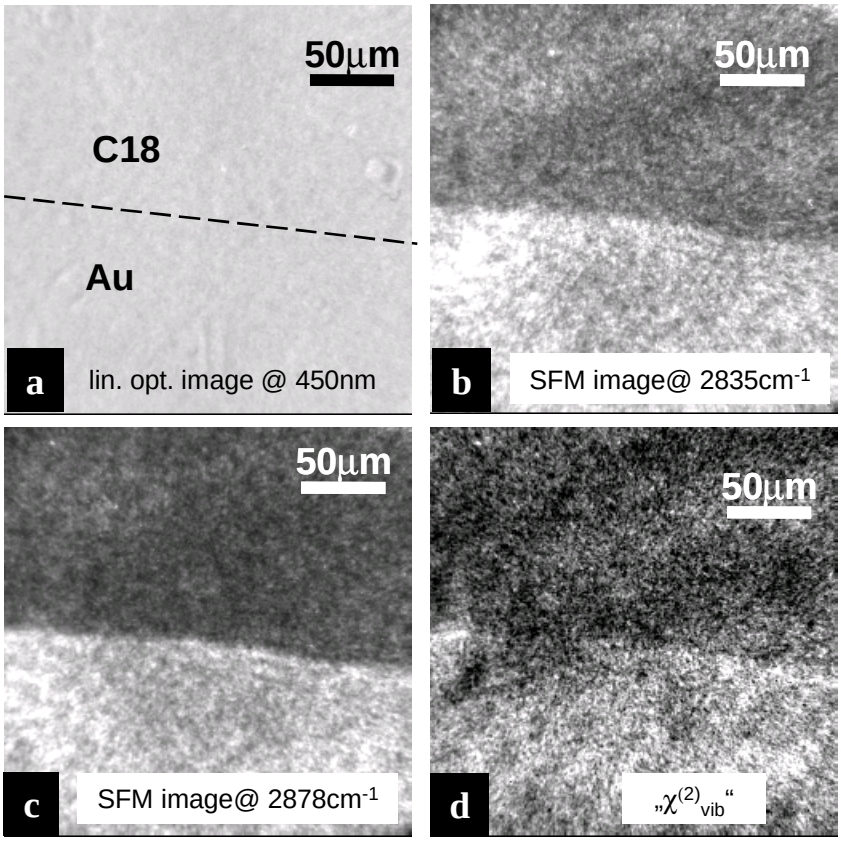

Figure 8: a) Linear image (λ = 450 nm) of the same area as b-d. The line marks the edge of the printed region, b) Electronic contrast: SFM image (80min) at 2835 cm^{-1}, c) SFM image (230min) at 2878cm^{-1}, d) Vibrational contrast (Details are given in the text). All images show exactly the same area. Image b and c are normalized with the acquisition time and they are displayed with an identical intensity scale.

4. CONCLUSIONS

We developed a sum frequency microscope for chemically selective and interface sensitive imaging of nontransparent samples like metals and semiconductors. Its performance is demonstrated by measurements of a laterally structured C18 thiolate self-assembled monolayer on Au. SFM images taken at resonant IR wavelengths show electronic and vibrational contrast between covered and uncovered regions of the substrate. Images taken at nonresonant IR wavelengths show electronic contrast. Evaluating both types of images allow for a separation of the different contributions to the effective second order nonlinear susceptibility. Mapping of the chemical composition on a surface is demonstrated.

REFERENCES

1. A. Zumbusch, G.R. Holtom, and X.S. Xie, „Three-Dimensional Vibrational Imaging by Coherent Anti-stokes Raman Scattering“, Phys.Rev.Lett. 82 (20), 4142 (1999)

2. M. Flörsheimer, C. Brillert, and H. Fuchs, „Chemical imaging of interfaces by sum-frequency generation“, Mater. Sci. Eng. C **8-9**, 335 (1999)
3. J. Squier and M. Müller, “High resolution nonlinear microscopy: A review of sources and methods for achieving optimal imaging”, Rev.Sci.Instr. **72** (7), 2855-2867 (2001)
4. Y. Shen, J. Swiatkiewicz, J. Winiarz, P. Markowicz, and P.N. Prasad, “Second-harmonic and sum-frequency imaging of organic nanocrystals with photon scanning tunneling microscope”, Appl.Phys.Lett. **77** (19), 2946 (2000)
5. B. Humbert, J. Grausem, A. Burneau, M. Spajer, and A. Tadjeddine, “Step towards sum frequency generation spectromicroscopy at a submicronic spatial resolution”, Appl.Phys.Lett. **78** (1), 135 (2001).
6. R.D. Schaller and J. Saykally, “Near-Field Infrared Sum-Frequency Generation Imaging of Chemical Vapor Deposited Zinc Selenide”, Langmuir **17** (7), 2055(2001)
7. Y. R. Shen, “Surface properties probed by SHG”, Nature **337**, 519, (1989); *The Principles of Nonlinear Optics*, Wiley, New York, (1984)
8. C. Hirose, N. Akamatsu, and K. Domen, Applied Spectroscopy **46**, 1051, (1992)
9. H.J. Krause and W. Daum, “High-power source of coherent picosecond light-pulses tunable from 0.41 to 12.9-mu-m, Appl.Phys.B **56** (1), 8 (1993).
10. J.C. Chastang, “Oblique viewing attachment for microscope”, Proceedings of the SPIE **399**, 239 (1983).
11. D. M.P. Hoffmann, K. Kuhnke, and K. Kern, submitted
12. A. Kumar, H.A Biebuyck, and G.M Whitesides, “Patterning Self-Assembled Monolayers: Applications in Materials Sciences”, Langmuir 10, 1498, (1994)
13. R. Ulmann, *An Introduction to Ultrathin Organic Films: From Langmuir Blodgett to Self-Assembly*, Academic Press, London, (1991)
14. F. Schreiber, “Structure and Growth of Self-Assembling Monolayers”, Progress in Surface Science **65**, 151, (2000)
15. P.L. Laibinis, G. M. Whitesides, D.L. Allara, Y. Tao, A.N Parikh, and R.G. Nuzzo, “Comparison of the Structures and Wetting Properties of Self-Assembled Monolayers of n-Alkanethiols on the Coinage Metal Surfaces, Cu, Ag, Au”, J.Am.Chem.Soc. **113**, 7152, (1991)
16. A. Le Rille, A. Tadjeddine, W. Zheng, and A. Peremans, “Vibrational spectroscopy of a Au(hkl)-electrolyte interface by in situ visible-infrared difference frequency generation”, Chem. Phys. Lett. **271**, 95 (1997)
17. M. Buck, F. Eisert, J. Fischer, M. Grunze, and F. Träger, “Investigation of Self-Organizing Thiol Films by Optical Second Harmonic Generation and X-Ray Photoelectron Spectroscopy“, Appl.Phys.A **53**, 552, (1991)
18. P. Guyot-Sionnest, J. Hunt, and Y. Shen,”Sum-frequency vibrational spectroscopy of a Langmuir film: Study of molecular orientation of a two-dimensional system”, Phys. Rev. Lett. **59**, 1597 (1987)